Meandered versus Spiral Novel Miniature PIFAs Implanted in the Human Head: Tuning and Performance

Asimina Kiourti and Konstantina S. Nikita

National Technical University of Athens, School of Electrical and Computer Engineering
akiourti@biosim.ntua.gr, knikita@ece.ntua.gr

Abstract. A meandered and a spiral stacked circular planar inverted–F antennas (PIFAs) are proposed for integration into head–implantable biomedical devices and wireless biotelemetry in the 402–405 MHz Medical Implant Communications Service (MICS) band. Designs only differ in the patch shape, feed, and shorting pin positions, while emphasis is given on miniaturization and biocompatibility. Phantom–related resonance detuning issues are addressed, and the PIFAs' radiation performance (radiation pattern, specific absorption rate (SAR) conformance with international guidelines, SAR distribution, and quality of up–link communication with exterior monitoring equipment) is evaluated and compared. Finite Difference Time Domain (FDTD) numerical simulations are performed.

Keywords: Biocompatibility, implanted biomedical devices, meandered antenna, medical implant communications service (MICS) band, spiral antenna.

1 Introduction

Wireless biomedical telemetry between implantable and exterior medical devices is an area of growing scientific interest [1]. In the most common scenario, the signals are transmitted wirelessly by means of antennas operating in the 402–405 MHz Medical Implant Communications Service (MICS) band, which is allocated for ultra–low–power active medical implants [2]. Miniaturization, biocompatibility, patient safety and quality of communication issues make the design of implantable antennas highly challenging.

In this study, we propose a meandered and a spiral MICS stacked planar inverted–F antennas (PIFAs) intended for integration into head–implantable biomedical devices (e.g. intra–cranial pressure sensors used in neurosurgery and neurology, brain–edema monitors for the paralyzed, position trackers for people with Alzheimer's disease etc). Microstrip designs are chosen because of their flexibility in design, conformability and shape, while shorting pins, high dielectric constant materials and surface optimization (meandering/spiraling) techniques are applied to increase the apparent size and reduce the physical dimensions of the structures. The proposed antennas are round–shaped, biocompatible, and identically–sized, achieving significant miniaturization compared to previously related works (e.g. [1], [3]–[7]). Tuning refinement is performed inside the skin tissue of a 15–tissue anatomical head

K.S. Nikita et al. (Eds.): MobiHealth 2011, LNICST 83, pp. 80–87, 2012.

model, and the radiation performance of the antennas (radiation pattern, specific absorption rate (SAR) conformance with international guidelines, SAR distribution, and quality of up–link communication with exterior monitoring equipment) is evaluated and compared. Finite Difference Time Domain (FDTD) numerical simulations are conducted in the XFDTD electromagnetic solver [8].

The paper is organized as follows. Section 2 presents the simulation set–ups and geometries of the proposed PIFAs. In Section 3, FDTD numerical results are presented regarding the performance of the proposed PIFAs implanted inside a 15–tissue anatomical head model. The paper concludes in Section 4.

2 Antenna Design

Since antennas are intended for skin tissue implantation, they are initially designed while in the center of a skin tissue simulating cube (Fig. 1(a)) (*initial PIFAs*) in order to speed–up the design process. Implantation and design refinement inside the skin tissue of a 15–tissue anatomical head model (Fig. 1(b)) are subsequently performed (*refined PIFAs*) [9], [10]. Tissue dielectric properties at 402 MHz are considered [11], while tissue mass densities are obtained from [9]. FDTD cells of $0.1 \times 0.1 \times 0.05$ mm^3, $2.5 \times 2.5 \times 2.5$ mm^3, $1.25 \times 1.25 \times 1.25$ mm^3 and $10 \times 10 \times 10$ mm^3 are used for the antenna, skin box, head model and free–space, respectively, in order to provide a high degree of spatial resolution in the simulations. Meshing is adaptive to avoid abrupt transitions. Free–space surrounds both simulation setups by 200 mm ($\lambda_0/4 \approx$ 186.5 mm, where λ_0 is the free–space wavelength at 402 MHz), and Liao absorbing conditions are considered in the boundaries to extend radiation infinitely far into space.

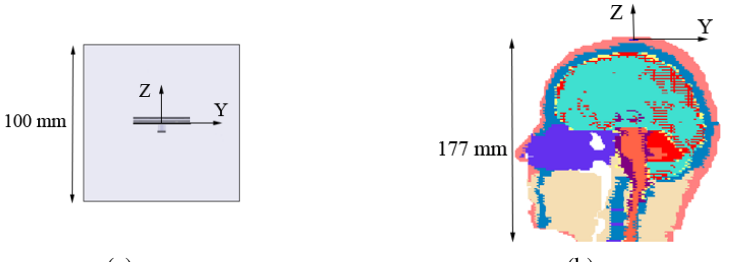

Fig. 1. Simulation set–ups: (a) skin tissue simulating cube, and (b) 15–tissue anatomical head

The proposed PIFA configurations are shown in Fig. 2. Antennas consist of a 4 mm–radius circular ground plane, and two identical stacked patches, relatively rotated by 180°. Both patches are fed by a 50 Ohm–coaxial cable (F) and radiate. Meandering/spiraling, patch stacking and shorting of the ground plane with the lower patch through a 0.2 mm–radius pin (S) lengthen the effective current flow path and miniaturize the PIFAs. Patches are printed on 0.25 mm–thick biocompatible alumina ($\varepsilon_r = 9.4$, $\tan\delta = 0.006$) substrates, while a 0.15 mm–thick alumina superstrate covers

the structures to preserve their biocompatibility and robustness. Throughout this study, the origin of the coordinate system is assumed to be at the center of the PIFAs' ground plane.

Designs of the proposed antennas were numerically studied and iterative simulation tests were performed to achieve the optimum resonance characteristics. The initial meandered PIFA has been presented by the authors in [9]. To obtain the initial spiral PIFA, patches are replaced by archimedean, single–arm, 1.9–turn spirals (inner radius of 1.1 mm), and the feed (F) and shorting pin (S) are re-positioned at (0 mm, 0 mm) and (3 mm, –1.5 mm), respectively. Tuning refinement is performed by suitably modifying the patch shapes while keeping all other PIFA design parameters constant. The refined meandered PIFA has meanders 1 and 5 (Fig. 2(b), (c)) lengthened by 0.5 mm, while patches are replaced by 1.95–turn archimedean spirals (inner radius of 1.05 mm) to obtain the refined spiral PIFA. The proposed designs achieve significant miniaturization compared to previously reported implantable PIFAs operating in the MICS band (e.g. [1], [3]–[7]), as indicated in Table 1.

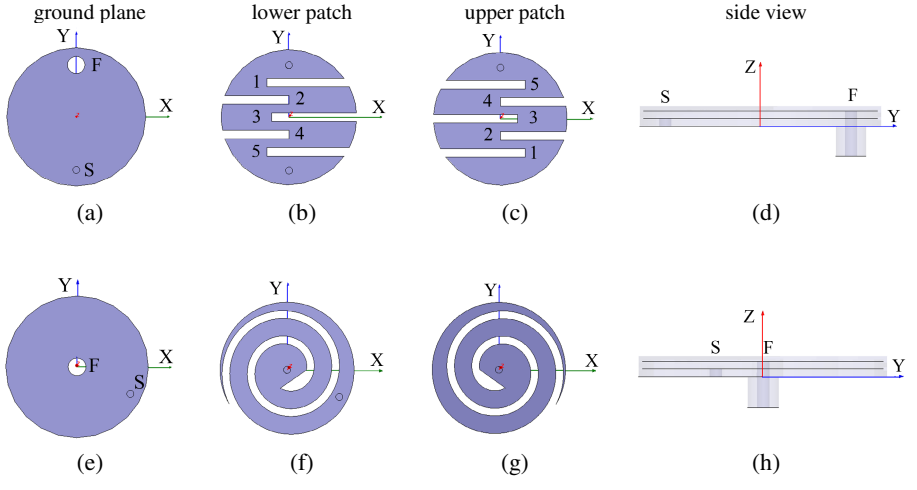

Fig. 2. Configurations of the proposed (a)–(d) meandered, and (e)–(h) spiral PIFAs

Table 1. Size comparison between the proposed and previously reported implantable PIFAs operating in the MICS band

PIFA	Volume occupied [mm^3]
[1]	$24 \times 32 \times 4 = 3072$
[3]	$22.5 \times 18.5 \times 1.9 = 790.9$
[4]	$23 \times 23 \times 1.25 \approx 661.3$
[5]	$\pi \times 7.5^2 \times 1.9 \approx 335.76$
[6]	$\pi \times 5^2 \times 1.815 \approx 142.6$
[7]	$8 \times 8 \times 1.9 = 121.6$
proposed	$\pi \times 4^2 \times 0.65 \approx 32.7$

3 Results and Discussion

3.1 Resonance Characteristics

Reflection coefficient ($|S_{11}|$) frequency responses of the proposed refined PIFAs implanted inside the anatomical head model are shown in Fig. 3. Even though the initial PIFAs are designed to resonate at 402 MHz while in the skin tissue simulating box, head implantation results in resonance frequency detunings by 11 and 5 MHz for the meandered and spiral PIFAs, respectively (solid). Detuning is attributed to the inherent dielectric loading of the surrounding tissues and exterior air on the antennas [9], [10], and is rectified by adequately modifying the patch shapes. Refined PIFAs resonate at 402 MHz when implanted inside the anatomical head model with broad 10 dB–bandwidths of 37 and 33 MHz, respectively (dotted).

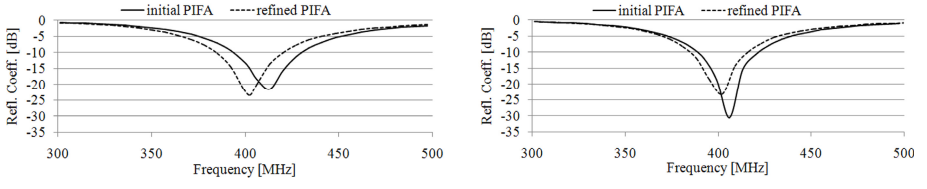

Fig. 3. Reflection coefficient ($|S_{11}|$) frequency responses of the (a) meandered, and (b) spiral PIFAs inside the anatomical head model

3.2 Far–Field Radiation Pattern

The 3D far–field gain radiation patterns of the refined PIFAs implanted inside the anatomical head model are shown in Fig. 4. Since the antennas are electrically very small, nearly omni–directional radiation is achieved. Comparable maximum gain values of –42.4 dB (in the $(\theta, \varphi) = (115^{o}, 95^{o})$ direction, where θ and φ are the zenith and azimuth angles, respectively) and –42.9 dB (in the $(\theta, \varphi) = (95^{o}, 270^{o})$ direction) are recorded for the meandered and spiral PIFAs, respectively. Low gain values are attributed to the miniaturized PIFA dimensions and human tissue absorption.

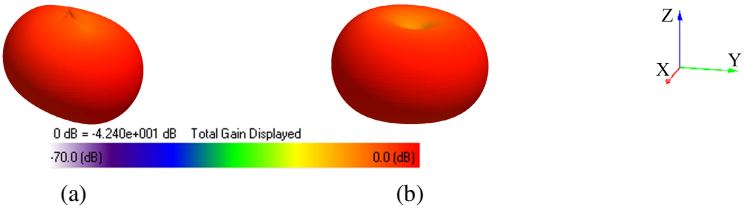

Fig. 4. Far–field gain radiation patterns of the refined (a) meandered, and (b) spiral PIFAs inside the anatomical head model

3.3 Specific Absorption Rate (SAR) Restrictions and Distribution

In order to ensure patient safety, the IEEE C95.1–1999 standard restricts the maximum SAR averaged over 1 g of tissue to less than 1.6 W/kg (1 g–avg SAR < 1.6 W/kg) [12], while the IEEE C95.1–2005 standard restricts the maximum SAR averaged over 10 g of tissue to less than 2 W/kg (10 g–avg SAR < 2 W/kg) [13]. Assuming a net–input power of 1 W incident to the proposed refined PIFAs, the maximum 1 g–avg and 10 g–avg SAR values induced in the anatomical head model are recorded (Table 2). Mass averaging procedures recommended by IEEE are applied [14]. The maximum allowed net–input power levels (P_{max}) which guarantee conformance with both IEEE standards are also given, indicating that the IEEE C95.1–1999 standard is much stricter.

Table 2. Maximum SAR values and power restrictions (P_{max}) for the refined PIFAs inside the anatomical head model

	Meandered PIFA	Spiral PIFA
1–g avg SAR	666.13 W/kg	676.01 W/kg
10–g avg SAR	80.21 W/kg	81.37 W/kg
P_{max} (IEEE C95.1–1999) [12]	2.402 mW	2.367 mW
P_{max} (IEEE C95.1–2005) [13]	24.93 mW	24.58 mW

Similar local SAR distributions are induced by the meandered and spiral PIFAs in the surrounding tissues, as indicated in Fig. 5 (the slices where maximum local SAR values have been calculated are depicted). To satisfy the strictest SAR limitations set by the IEEE guidelines, the net input power has been set to 2.402 mW and 2.367 mW for the meandered and spiral PIFAs, respectively (Table 2). For comparison reasons, all local SAR results have been normalized to 2 W/kg.

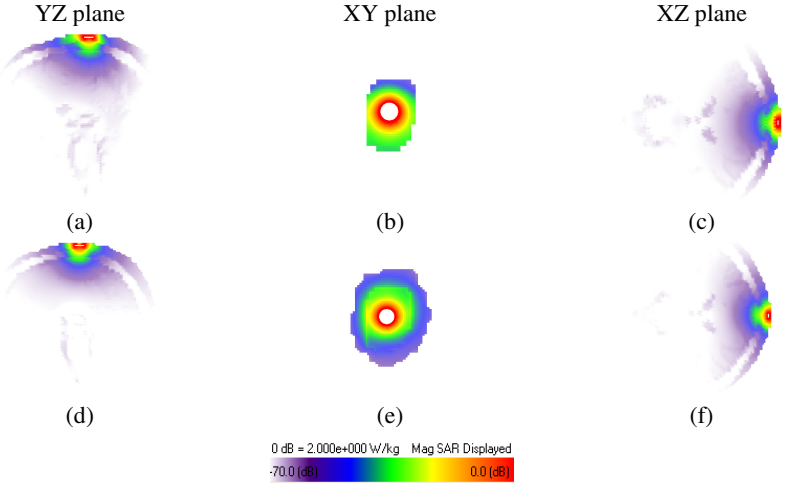

Fig. 5. Distribution of the local SAR on the YZ, XY and XZ slices of the anatomical head model where maximum local SAR values have been calculated for the (a)–(c) meandered (net input power = 2.402 mW) and (d)–(f) spiral (net input power = 2.367 mW) PIFAs

3.4 Quality of Up–Link Communication

The quality of the wireless communication up–link which is formed between the proposed refined PIFAs implanted inside the anatomical head model (transmitter) and exterior monitoring equipment (receiver) is assessed. A simplified half–wavelength ($\lambda_0/2$, f_0 = 402 MHz) dipole antenna, placed vertically and symmetrically around the y–axis (i.e. centered at (θ, φ) = (90°, 270°)), is considered to account for the exterior receiving antenna (Fig. 6(a)).

The transmission performance of the meandered and spiral PIFAs is shown in Fig. 6(b) in terms of the simulated transmission coefficient ($|S_{21}|$) versus distance between the antennas (d). The transmission coefficient, $|S_{21}|$, quantifies power transmission in the wireless link, so that $|S_{21}|^2 = P_r/P_t$, where P_t is the available power at the transmitter, and P_r is the power delivered to a 50 Ohm–load terminating the receiver antenna [15]. Higher $|S_{21}|$ values for the spiral PIFA are attributed to its higher far–field gain value in the (θ, φ) = (90°, 270°) direction (–42.92 dB), as compared to that of the meandered PIFA in the same direction (–44.68 dB).

The dependence of P_r on the transmitter–receiver distance (d) is shown in Fig. 6(c). Net input powers of 2.402 mW (P_t = 2.412 mW or 3.823 dBm) and 2.367 mW (P_t = 2.397 mW or 3.798 dBm) are considered for the meandered and spiral PIFAs, respectively, in order to satisfy the strictest IEEE limitations for the SAR (Table 2). Assuming the most distal scenario of this study (d = 1 m), the exterior receiver should have enough sensitivity to detect the signal from the implanted device which is as weak as –63.04 dBm and –58.62 dBm for the meandered and spiral PIFAs, respectively.

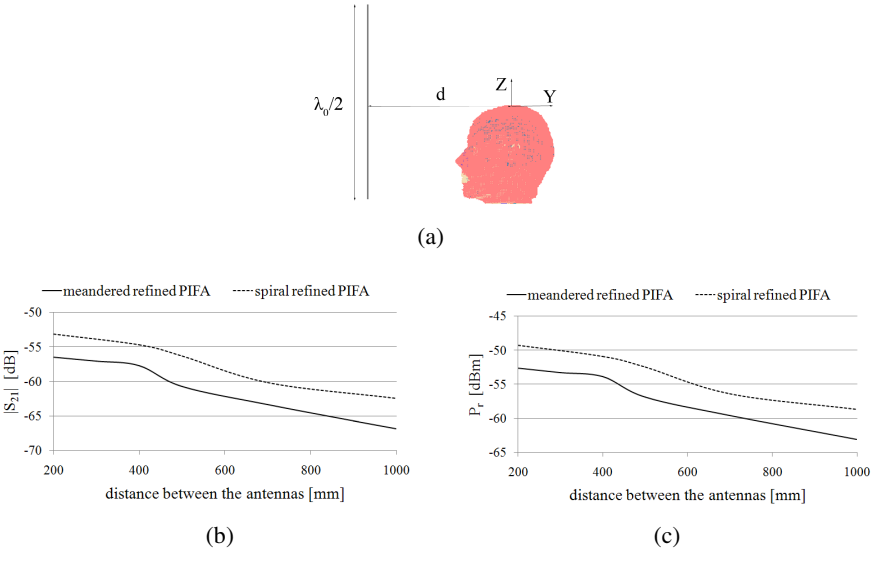

Fig. 6. (a) Transmission scenario simulation set–up, (b) transmission coefficient ($|S_{21}|$) of the refined PIFAs and (c) power delivered to the receiver antenna (P_r) versus distance between the antennas (d)

4 Conclusion

Meandering and spiraling techniques were applied to design two identically–sized MICS miniature PIFAs for integration into head–implantable biomedical devices. Phantom–related resonance detuning issues were addressed, and design modifications were proposed to refine tuning of the PIFAs when implanted inside a 15–tissue anatomical head model. Based on FDTD simulations, the performance of the antennas (exhibited far–field radiation pattern, SAR conformance with international guidelines, SAR distribution, and quality of up–link communication with exterior monitoring equipment) was assessed and found to be highly comparable.

Future work will include application of optimization algorithms to optimally tune the PIFAs inside the 15–tissue anatomical head model. Subsequent investigations will also include fabrication of the proposed antennas and experimental validation of the simulation results.

References

1. Kim, J., Rahmat–Samii, Y.: Implanted Antennas Inside a Human Body: Simulations, Designs and Characterizations. IEEE Transactions on Microwave Theory and Techniques 52, 1934–1943 (2005)
2. Medical implant communications service (MICS) federal register. Rules Reg. 64, 69926–69934 (1999)
3. Lee, C.M., Yo, T.C., Huand, F.J., Luo, C.H.: Bandwidth enhancement of planar inverted–F antenna for implantable biotelemetry. Microwave and Optical Technology Letters 51, 749–752 (2009)
4. Karacolak, T., Cooper, R., Topsakal, E.: Electrical properties of rat skin and design of implantable antennas for medical wireless telemetry. IEEE Transactions on Antennas and Propagation 57, 2806–2812 (2009)
5. Lee, V.M., Yo, T.C., Luo, C.H.: Compact broadband stacked implantable antenna for biotelemetry with medical devices. In: IEEE Annual Wireless and Microwave Technology Conference (2006)
6. Liu, W.C., Chen, C.H., Wu, C.M.: Implantable Broadband Circular Stacked PIFA for Biotelemetry Communication. Journal of Electromagnetic Waves and Applications 22, 1791–1800 (2008)
7. Liu, W.C., Yeh, F.M., Ghavami, M.: Miniaturized Implantable Broadband Antenna for Biotelemetry Communication. Microwave and Optical Technology Letters 50, 2407–2409 (2008)
8. XFDTD, Electromagnetic Solver Based on the Finite Difference Time Domain Method, Remcom Inc.
9. Kiourti, A., Christopoulou, M., Nikita, K.S.: Performance of a Novel Miniature Antenna Implanted in the Human Head for Wireless Biotelemetry. In: 2011 IEEE International Symposium on Antennas and Propagation (2011)
10. Kiourti, A., Christopoulou, M., Koulouridis, S., Nikita, K.S.: Design of a Novel Miniaturized Implantable PIFA for Biomedical Telemetry. In: Lin, J., Nikita, K.S. (eds.) MobiHealth 2010. LNICST, vol. 55, pp. 127–134. Springer, Heidelberg (2011)
11. Gabriel, C., et al.: The Dielectric Properties of Biological Tissues. Physics in Medicine and Biology 41, 2231–2293 (1996)

12. IEEE, Standard for Safety Levels with Respect to Human Exposure to Radio Frequency Electromagnetic Fields, 3kHz to 300GHz. IEEE Standard C95.1–1999 (1999)
13. IEEE, Standard for Safety Levels with Respect to Human Exposure to Radio Frequency Electromagnetic Fields, 3kHz to 300GHz. IEEE Standard C95.1–2005 (2005)
14. IEEE, Recommended Practice for Measurements and Computations of Radio Frequency Electromagnetic Fields with Respect to Human Exposure to such Field, 100 kHz to 300 GHz. IEEE Standard C95.3–2002 (2002)
15. Warty, R., Tofighi, M.R., Kawoos, U., Rosen, A.: Characterization of implantable antennas for intracranial pressure monitoring: reflection by and transmission through a scalp phantom. IEEE Transactions on Microwave Theory and Techniques 56, 2366–2376 (2008)